The Process of Formation of Non-Spherical Nanoparticles -Application to Gold Nanorods-

The process of formation of gold nanorods with aspect ratios (ARs, ratio of long axis to short axis) of 2, 4, and 6 was investigated by time-resolved distance distribution functions calculated from small-angle X-ray scattering profiles. The growth in nanorod length as a function of the reaction time was determined without having to approximate or simplify the actual nanorod shape. The mechanism of the variation in the ARs of the formed nanorods is evaluated on the basis of growth rates for the length and the width, each considered individually.

In general, nanoparticles have spherical shape and symmetry. Nanorods are rod-shaped nanoparticles, and display unique optical properties due to their non-spherical shape and tunable longitudinal surface plasmon resonance (SPR) [1]. Beyond controlling the diameter of spherical nanocrystals, an ability to control the shape of nanorods would greatly assist in tuning their properties. The wavelength of light absorbed by gold nanorod SPR surprisingly shifts from 520 nm (spherical gold nanoparticles) to the infrared region, depending on the shape.

Small-angle X-ray scattering (SAXS) experiments yield decisive information on the structure of nanoparticles. Here, we report on the process of formation of gold nanorods, studied by time-resolved distance distribution functions $P(r)$ calculated by Fourier transform of the overall SAXS profile [2]. $P(r)$ gives the most reliable information on the structure of a scattering center (that is, a scatterer) in real space, because no approximations or assumptions are used in the function. The value of r at which $P(r) = 0$ is exactly equal to the maximum length of the scatterer. For nanorods, the maximum length reliably corresponds to the major-axis length, even though other different-shaped particles, such as cubic and spherical nanoparticles, exist in the system [3]. An understanding of the growth kinetics of nanomaterials during chemical synthesis is essential for the development of structural controls and synthesis methods.

SAXS experiments were performed at BL-15A. We newly constructed the following apparatus for the simultaneous measurement of SAXS and UV-vis-NIR absorption spectra: (1) a sample holder made entirely of titanium, (2) a frame-moving detector using an imaging plate with long detectable area, and (3) a direct beam monitor sensor using a photo diode [2, 6].

We prepared gold nanorods using a seed-mediated growth method [4, 5]. To generate nanorods with aspect ratios (ARs, ratio of long axis to short axis) of 2 and 4, we prepared a growth solution containing 5.0 mL of $HAuCl_4$ (1.0 mM) and 5.0 mL of cetyltrimethylammonium bromide (CTAB, 0.20 M). To this solution, we added 50 and 200 μL of $AgNO_3$ (4.0 mM) for ARs 2 and 4, respectively, and then we mixed 110 μL of ascorbic acid (78.8 mM) and 100 μL of seed (0.236 mM as gold content) into the respective solutions. To generate nanorods with AR 6, we prepared a growth solution of 5.0 mL of benzyldimethylhexadecylammonium chloride (BDAC) plus CTAB as surfactant (in a BDAC/CTAB molar ratio of 2.5), to which we added 5.0 mL of $HAuCl_4$ (1.0 mM) and 200 μL of $AgNO_3$ (4.0 mM). Into the solution, we mixed 80 μL of ascorbic acid (78.8 mM) and 100 μL of seed (0.236 mM as gold content). In synthesizing nanorods with ARs of 2 and 4, the method enables us to control the length of a nanorod by changing the silver ion content in the growth solution. For AR 6 nanorods, we used additional surfactant.

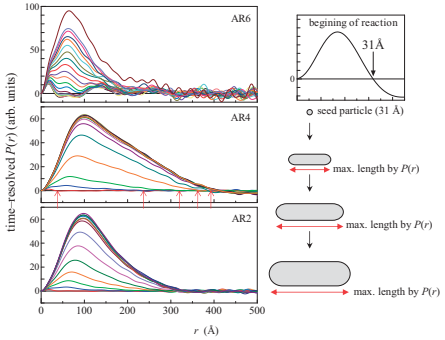

Figure 1
Time-resolved distance distribution functions $P(r)$. Arrows in the figure for AR 4 indicate the maximum length at each reaction time. The right-hand side of the figure shows the formation process of the nanorods. $P(r)$ of the seed spherical particle is also shown and the axes are the same as the left-hand side figure. The maximum lengths evaluated by $P(r)$ exactly correspond to the major-axis lengths of the growth.

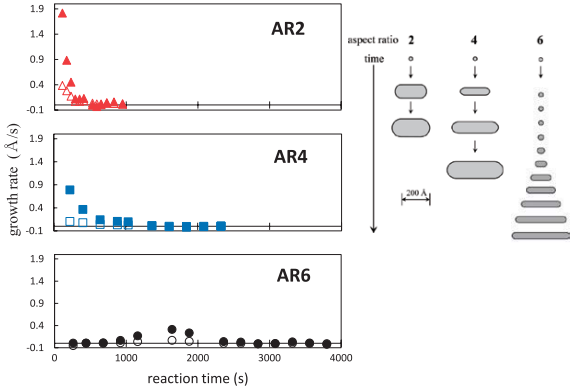

Figure 2
Growth rates for ARs of 2, 4, and 6 as a function of reaction time. Solid and open symbols refer to changes in length and width, respectively. Combining the absorption spectral data with the maximum length obtained by $P(r)$, the length and width growth rates are evaluated, each considered individually. The right-hand side of the figure shows the growth kinetics for the variation in the aspect ratios of the formed nanorods, obtained from the time dependence on growth rate.

Time-resolved distance distribution functions $P(r)$ are shown in Fig. 1 as a function of reaction time. As mentioned above, the value of r at which $P(r) = 0$ corresponds to nanorod length. $P(r)$ at the beginning of the reaction is also shown on the right-hand side of the figure. The profile indicates that the seed particles have a spherical shape and the size is estimated to be 31 Å. The progress of growth from seed particle to nanorod is precisely observed from the change in $P(r)$, especially for AR 6.

Combining the UV-vis-NIR spectral data with the maximum length, the length and width growth rates are evaluated, each considered individually. Figure 2 shows the growth rates as a function of the reaction time. At the beginning of the reaction, the length growth rate for AR 2 is larger (by a factor of 2.3) than that for AR 4. The width growth rate for AR 2 is much larger (by a factor of 4.0) than that for AR 4. In contrast, the ratio of length growth rate to width growth rate shows the opposite trend: the ratio for AR 2 is smaller than that for AR 4. On the other hand, the nucleation process will occur in the solution up to 1000 s in AR 6 nanorod synthesis, since the growth rates gradually increase with the reaction time. The following tendencies are evident as shown in the right-hand side of Fig. 2. (1) For AR 2, both length growth rate and width growth rate are large. (2) For AR 4, the length growth rate is greater than the width growth rate, and so a longer rod is formed. (3) Reaction rates descend in the following order of aspect ratio: 2 > 4 >> 6.

REFERENCES

[1] C.J. Murphy, T.K. Sau, A.M. Gole, C.J. Orendorff, J. Gao, L. Gou, S.E. Hunyadi and T. Li, *J. Phys. Chem. B* **109** (2005) 13857.
[2] T. Morita, E. Tanaka, Y. Inagaki, H. Hotta, R. Shingai, Y. Hatakeyama, K. Nishikawa, H. Murai, H. Nakano and K. Hino, *J. Phys. Chem. C* **114** (2010) 3804.
[3] T. Morita, Y. Hatakeyama, K. Nishikawa, E. Tanaka, R. Shingai, H. Murai, H. Nakano and K. Hino, *Chem. Phys.* **364** (2009) 14.
[4] N.R. Jana, L. Gearheart and C.J. Murphy, *Adv. Mater.* **13** (2001) 1389.
[5] B. Nikoobakht and M.A. El-Sayed, *Chem. Mater.* **15** (2003) 1957.
[6] T. Morita, Y. Tanaka, K. Ito, Y. Takahashi and K. Nishikawa, *J. Appl. Cryst.* **40** (2007) 791.

BEAMLINE

15A

T. Morita[1, 2], E. Tanaka[2], H. Hotta[2], R. Shingai[2], Y. Hatakeyama[1], K. Nishikawa[1] and K. Hino[2] ([1]Chiba Univ., [2]Aichi Univ. of Education)